Hindawi Publishing Corporation
Journal of Nanotechnology
Volume 2012, Article ID 545930, 14 pages
doi:10.1155/2012/545930

Research Article

The Optimum Dispersion of Carbon Nanotubes for Epoxy Nanocomposites: Evolution of the Particle Size Distribution by Ultrasonic Treatment

Tomas Roll Frømyr,[1,2] Finn Knut Hansen,[1,2] and Torbjørn Olsen[1]

[1] *Norwegian Defence Research Establishment, P.O. Box 25, 2027 Kjeller, Norway*
[2] *Department of Chemistry, University of Oslo, P.O. Box 1033, Blindern, 0315 Oslo, Norway*

Correspondence should be addressed to Finn Knut Hansen, f.k.hansen@kjemi.uio.no

Received 9 March 2012; Accepted 23 April 2012

Academic Editor: Huisheng Peng

The ultrasonic dispersion of multiwalled carbon nanotube (MWCNT) suspensions was assessed by studying the differential sedimentation of the particles in an acid anhydride often employed as a curing agent for epoxy resins. The particle size distributions were characterized by the means of a disc centrifuge, and the effect of dispersion time, power density, and total energy input, for both bath and circulation probe ultrasonic dispersing equipment was investigated. The mass of freely suspended MWCNTs relative to agglomerated MWCNTs was estimated as a measure of the quality of the dispersions, and the results showed that this ratio followed a power law scaling with the energy dissipated in the sonication treatment. If the sonication power level was too high, sonochemical degradation of the curing agent could occur. The mean agglomerate MWCNT size distribution was estimated, and the fragmentation of the agglomerates was modeled by means of fragmentation theory. Indications of both rupture and erosion fragmentation processes for the MWCNT agglomerates were observed.

1. Introduction

Carbon nanotubes (CNTs) have been studied extensively since the landmark paper by Iijima in 1991 [1]. The exceptional mechanical, thermal, and electrical properties combined with the high aspect ratio and large surface area have made CNTs a promising material for a wide range of applications. However, there are major challenges to overcome in order to utilize these properties. There are several different production methods for CNTs, such as laser ablation, electrolysis, electric arc discharge, sonochemistry, chemical vapour deposition, and catalyst arrays [2]. These methods produce different CNTs with different chemical structure, length, diameter, defects, and varying types and degrees of contamination [3]. This will affect physical properties, such as differences in nanotube curvature, reactivity, failure mechanisms, mechanical properties, and surface interactions.

Although the mechanical properties of carbon nanotubes are superior to, for example, continuous and short carbon fibres, problems with dispersion, load transfer, and alignment in a polymer matrix have, so far, not led to CNT composites being a competitive alternative to these more traditional materials. Carbon-fibre-reinforced polymers (CFRPs) are more suitable for use in structural composites. The primary role of a polymer matrix is to hold the fibres in plane and transfer load, but there are modes of deformation where an increase in the mechanical properties of the polymer matrix is of importance. In this context, CNTs have been considered as a reinforcing material with a random orientation similar to conventional short fibre reinforced composites [4–6]. However, to achieve any form of reinforcement effect, processing challenges such as poor wettability, heavy aggregation, and viscosity build up in dispersions of even low concentrations must be overcome [7]. In order to obtain improvement of the composites mechanical properties, the interfacial shear strength between the CNTs and polymer matrix should be maximized to transfer the load to the reinforcing particles [8]. Studies have shown

that the load transfer between individual nanotubes is low [9], probably because of slippage between them, and that larger agglomerates have poor mechanical properties [10]. To achieve good dispersions, with a minimal amount of agglomerates, is therefore of vital importance to minimize these effects and to optimize the CNT-matrix interface for improved load transfer.

Several different dispersion methods have been suggested for carbon nanotubes. In high viscosity systems, such as epoxy resins, calendaring, milling, grinding, high speed shear mixing, high-pressure homogenization, and sonication have been used [11, 12]. Sonication, which is the most commonly reported method, is a process where a transducer is used to irradiate a liquid with a high pressure sound field with the result of growth of cavities which implode with a violent and localised release of energy. In a bath-type sonicator the sound field is close to uniform, and the treatment of the suspension is equally homogenous. Unfortunately, the sound pressure in a bath sonicator is low compared to a horn, that is, tip sonicator. Tip sonicators can generate large sound pressures by connecting the transducer to a resonating metal rod. A high-intensity sound field is generated at the end of the rod, inducing mixing by turbulent fluxes and acoustic streaming in suspensions [13]. Furthermore, ultrasonic cavitation can also produce high-energy inter-particle collisions and particle surface damage caused by implosion shock waves and micro jets [14].

These effects lead to the fragmentation of agglomerates in the suspension [15], and are quite effective at treating smaller volumes of low viscosity liquids. However, because of the localization of the high-energy sound field around the tip of the sonicator, stirring is normally needed for larger volumes to ensure a homogenous treatment of the entire sample. Dispersion in higher-viscosity liquids, such as polymers or prepolymers, is a more complex problem, in that the viscosity will also affect the cavitation of the liquid [13, 16]. One way to overcome this problem is to dilute the suspension with a liquid of lower viscosity; another way is to predisperse the particles in another liquid before mixing with the high-viscosity liquid [2, 17]. A typical problem with this approach is how to completely remove the excess solvent and how to avoid reagglomeration of CNTs during this removal. In composite materials production, a low molecular weight inert liquid is undesirable, because solvent residues may act as a softener in the matrix. Another processing route is, at least for low to medium viscosity systems, to use a flow cell and direct the flow of the suspension through the high-intensity sound field at the sonicator tip. Flow cells are available as standard equipment for most high power lab sonicators.

Dispersion, purification, and functionalization of carbon nanotubes have been investigated extensively. Characterization of the final dispersion is important, because the procedures developed for one type of CNT may be inappropriate for another. Common characterization techniques have been difficult to carry out on CNT suspensions, and the results are often ambiguous. Electrozone, light scattering, and different types of microscopy/image analysis methods are the main techniques for particle sizing in this size range, but they all have significant drawbacks. The electrozone method works well for insulating particles, but conducting nanotube poses problems. In addition, the interpretation of the signal for nonspherical particles is also a challenge. Flow particle image analysis (FPIA) has gained significant popularity in recent years because of the advances in electronics and computing power. However, single CNTs cannot be resolved by this method. Electron microscopy with image analysis works well in the whole size range, but samples must be deposited on a suitable surface and dried. This sample preparation may change the state of dispersion in the sample. The method is also very laborious, and statistically reliable data are difficult to obtain for very wide size distributions.

Static and/or dynamic light scattering (DLS) methods translate angular- and/or time-resolved light scattering to particle size distributions (PSD) with very good results for more or less monodispersed spherical particles. For CNTs, light-scattering theory for high-aspect ratio particles must be used to get reliable results [18, 19]. In addition, there are serious challenges with LS techniques when the particle distribution is wide, as is often the case with suspensions of heavy-agglomerated carbon nanotubes. Schaefer and Justice [20] used scattering techniques such as small-angle X-ray scattering (SAXS) and small-angle neutron scattering (SANS) along with ultra-small-angle X-ray scattering (USAXS) and ultra-small-angle neutron scattering (USANS) and correlated this to conventional light scattering. Advances in USANS in recent years have increased the signal-to-noise ratio significantly and made USANS particularly interesting. Still, both small-angle X-ray and neutron scattering demand specialized facilities and are hardly routine techniques. The inherent problem of scattering techniques is that spatial averaging leads to a loss of information. In broad and multimodal systems, the difference between real PSDs and data from scattering experiments can be significant. By using supporting optical and electron imaging techniques, model assumptions about the real PSD can be made. With these assumptions, the angular scattering intensities can be fitted to extract useful information about the sample mass distribution. Two problems arise: (1) sample preparation for imaging may drastically change the distribution, making the model assumptions needed for the scattering experiments erroneous, and (2) the sensitivity to changes in the PSD is low for broad and multimodal distributions, because the scattering efficiency changes significantly with size. Schaefer and Justice have partly, and cleverly, addressed problem number 2 by using data from different scattering techniques to study dispersions of carbon nanotubes. However, only average particle size ranges are discussed, because scattering techniques lack the resolution needed to construct a continuous PSD for dispersions of CNTs. Only coarse estimates of the degree of dispersion are possible, and the size and shape evolution of the submicron CNT agglomerate size distribution is not possible. Kim et al. [21] have shown that DLS can be used in conjunction with differential scanning calorimetry to assess the quality of dispersion in CNT-epoxy composites.

Different sedimentation techniques are known to be well suited for addressing the problem of wide size distributions. Ultracentrifugation with subsequent measurement of UV/vis transmittance of the suspension has been used to assess the

quality of dispersion [22], but time-resolved measurements of the light transmittance are necessary to obtain information of particle size distributions. Such information is available with an analytical centrifuge, where the transmittance measurements can be done in real time, while the sample is spinning [23]. Pegel et al. and others [12, 24–26] have shown that this technique can be applied to CNT suspensions. A more direct determination of the particle size distribution of CNT suspensions is *differential sedimentation particle size analysis* (DCP). This is a classical sizing technique which can be used to determine high-resolution size distribution data [27], and the most common instrument for this purpose is the analytic disk centrifuge (DCF). In this instrument, the particles settle in a liquid in a centrifugal field within a hollow disk. A small sample is deposited on the liquid surface, and the sedimentation time using a detector at the outer rim of the disc is recorded. Because larger particles have a shorter sedimentation time than smaller particles, the inherent size fractionation makes this method well suitable for wide distributions of particles with varying geometry. Recently, this technique has received attention for the analysis of CNT dispersions. The group of Nadler et al. [28] have shown the suitability of DCP in analysing dispersions of CNTs, and they have used the technique to compare the effectiveness of a bath sonicator with a three-roll mill. Typical particle size distributions show a bimodal shape with a mass fraction of free unentangled nanotubes and another mass fraction of entangled agglomerated CNTs [29]. In the work of Nadler et al., the separation of nanotubes from agglomerates was seen as an exfoliation process, and the mass percentage of exfoliated nanotubes was defined as the *degree of exfoliation* and determined directly from PSD data.

In this investigation we have studied the effects of sonication on the dispersion of multiwalled carbon nanotubes (MWCNTs) in an epoxy hardener. The advantage of this scheme is that the dispersion can be added directly to an epoxy resin, and cast without any solvent removal, to prepare nanoenforced epoxy composites. In order to stabilise the dispersions, a polymer stabiliser is added and care has been taken to treat the samples with reproducible homogenous sonication. The dispersions have been characterized using DCF and scanning electron microscopy (SEM).

2. Experimental

2.1. Materials. Multiwalled carbon nanotubes made by Arkema, Graphistrength C100, were obtained from Sigma-Aldrich. These nanotubes are made by catalytic chemical vapour deposition (CVD). According to the supplier, the carbon content is above 90% (w/w) and metallic impurities were below 10% (w/w). The outer diameter was 10–15 nm, and the inner diameter was 2–6 nm. The length range was 0.1–10 μm, and the wall thickness was reported to be 5–15 graphene layers. SEM images revealed that the supplied material consisted of agglomerated, highly entangled nanotubes, which is normal for CNTs produced by CVD. Moreover, the nanotubes had large curvatures, probably because of defects or a low degree of graphitization.

2.2. Dispersion. MWCNTs were dispersed in methyl tetrahydrophthalic anhydride (MTHPA, Aradur 917, Huntsman). MTHPA is a versatile epoxy curing agent that gives a long pot life and good mechanical properties with a suitable epoxy resin. It is a liquid with a relatively low viscosity at room temperature (50–100 mPas at 25°C), allowing for solvent free sonication with CNTs. Amine-based curing agents were also considered, as several of them exhibit low viscosity and do not react with water. Unfortunately, the mixing ratio between epoxy resin and amines is normally quite high, whereas MTHPA is typically mixed with epoxy resins in ratios close to 1 : 1. A lower-weight fraction of CNTs in the MTHPA curing agent is needed to reach a certain loading level in the cured epoxy, compared with amine-curing agents. Disperbyk 2150 (D 2150, Byk additives) was used as dispersing agent for the CNTs in MTHPA. D 2150 is a "solution of a block-copolymer with basic pigment affinic groups" according to the manufacturer. Supposedly, it is well suited for carbon particles in organic liquids, and has been used successfully for CNTs [28, 30, 31].

2.3. Ultrasonication. First, 3% (w/w) of D 2150 was dissolved in MTHPA, then 1% (w/w) of CNTs was added. Sonication was performed in either a bath ultrasonicator (Bandelin Sonorex Digital 10P, 352 kHz, 480 W) or a horn type ultrasonicator (Branson Digital Sonifier S-450D, 25 kHz, 400 W) with a flow cell attachment with a cooling jacket. A peristaltic pump (Watson Marlow 503U) with silicon tubing (8 mm outer diameter, 4.8 mm inner diameter, Watson Marlow) was used to generate the flow through the cell.

With the horn sonicator, both the effect of time and intensity of the sonication could be investigated. The energy delivered by the horn sonicator was controlled by changing the amplitude at the tip of the resonating horn. The sonicator control unit varies the power delivered to keep the oscillation of the horn tip at constant amplitude. Suspensions were run in a closed loop at different horn tip amplitudes, given as a percentage of the maximum tip amplitude of 145 μm. It was possible to operate the transducer at amplitudes up to 70% of the maximum value. The cooling jacket was water-cooled and held at 20°C. The temperature of the dispersion rose during sonication, but the maximum recorded temperature inside the flow cell was always below 50°C.

The bath sonicator, on the other hand, was run at maximum power in all experiments, since the intensity is low even at the 100% amplitude setting. The water level was kept at the recommended fill level, and the suspensions were completely immersed in the bath. The temperature equilibrated at approximately 50°C during bath sonication.

2.4. Characterization. The dispersions were characterised in a disc centrifuge (DCF) (DC24000, CPS instruments Inc.). The disc centrifuge operates by the principles of differential sedimentation, and a solution with a density gradient is needed for stable operation. A 5–15% (v/v) gradient of Halocarbon 1.8 (Solvadis) in methyl isobutyl ketone (MIBK) (>99% Merck) was created with a linear density gradient former (Beckmann) before each measurement.

The density gradient showed excellent baseline stability over several hours. The MTHPA dispersions were diluted 1 : 20 in MIBK, that is, 0.05% (w/w) CNT, and sonicated one minute in the bath sonicator immediately before analysis. 0.1 mL of the sample was injected and the DCF was run at 24000 rpm.

The disc centrifuge uses a detector with a 405 nm light source, and calculates the particle concentration from the transmittance of the light source. From (1), the turbidity (τ) is a function of the number of particles (N) in the light path, the particle's geometric cross-section (A), and the light extinction efficiency (Q_{ext})

$$\tau = NAQ_{\text{ext}}. \tag{1}$$

Both light absorption and elastic scattering are functions of both the particle diameter and its complex refractive index [32] and are accounted for in the term Q_{ext}. Given the refractive index, the instrument calculates Q_{ext} as a function of the particle size, assuming spherical particles. It then calculates the fractional mass distribution as a function of the particle size from the detector signal. Integrating the fractional mass, W_D, for a given size range gives the total particle mass within that range. The apparent Stokes equivalent spherical diameter, D_{ST}, of the particles is calculated from the sedimentation time. It is the equivalent diameter of a hard sphere with the same density, having the same sedimentation time as the measured particles. The resulting particle size distribution is a plot of W_D as a function of D_{ST}.

Drops of the diluted dispersions were also deposited on silicon wafers and dried. Electron micrographs of the surfaces were taken at low acceleration voltages in a field emission scanning electron microscope (Hitatchi SU-6600).

2.5. Thermogravimetric Analysis. To check for possible chemical reactions between the nanotubes and the other components in the dispersion or for excessive damage of the CNTs [33, 34], thermogravimetric analysis (TGA) was run on a TGA2950 Hi-Res instrument (TA instruments). A lowered oxidation onset temperature would indicate degradation of the nanotubes [35]. Prior to the analysis solvent was removed from the suspension by the following cleaning procedure: 1 g of suspension was diluted with 35 mL MIBK, then it was run for 1 min in the ultrasonic bath, and finally centrifuged, for 2 h at 30000 rpm (WX Ultra 80, Sorvall). The precipitate was dried in a vacuum oven at 60°C overnight before it was diluted once more, centrifuged, and dried, all under the same conditions. Approximately 5 mg of sample was deposited in a platinum cup and heated at 5°C/min in dynamic rate Hi-Res mode [36], where the heating rate is slowed down during significant changes in mass. The resolution is enhanced compared to constant heating at the same rate. Compressed air (AGA) at 100 mL/min was used as purge gas. The components of the suspension were analysed separately as a reference. No sample preparation was done prior to the TGA with these samples.

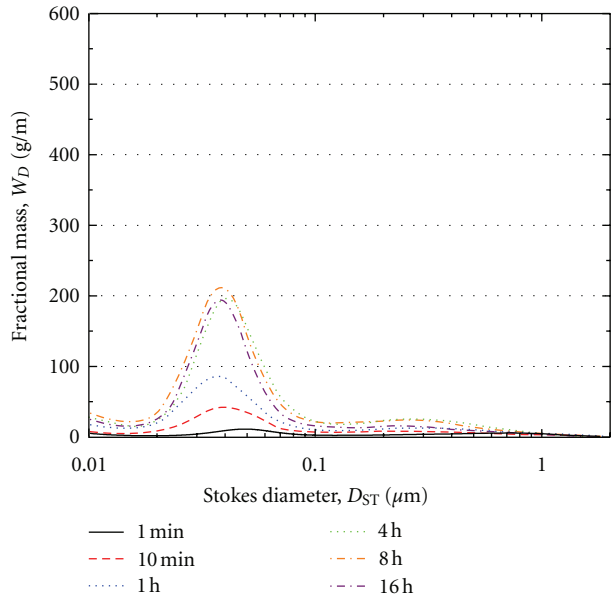

Figure 1: Particle size distributions of Arkema CNTs with increasing sonication time in an ultrasonic bath.

3. Results and Discussion

Broad bimodal particle size distributions were observed for all dispersions of CNTs. The distinct peaks in the distributions between 20 nm and 100 nm, shown in Figure 1, are attributed to the free, fully dispersed, that is, exfoliated, carbon nanotubes. The mass fractions above 100 nm are attributed to agglomerates of CNTs. This is in agreement with the previous observations of Nadler et al. [28].

There are indications of a mass fraction below 20 nm in the PSDs for the Arkema CNTs. Care must, however, be taken when interpreting data in this size range, as this signal may be an artefact due to drift in the baseline. To calculate the amount of particles in the suspension, the turbidity is divided by the light extinction efficiency, Q_{ext}, which approaches zero with decreasing particle size for small particles in the Rayleigh regime. A small drift in the turbidity baseline can occur, even though the baseline showed excellent stability throughout the experiments. The instrument calculates an initial linear baseline drift and compensates for this, but any change in the drift during an experiment remains uncorrected. Degradation of the density gradient in the spin fluid and temperature fluctuations within the instrument are the main causes for the instrument drift. For long sedimentation times, the drift can be nonlinear and significant. Hence, the instrument measures a small positive or negative signal and correlates this to a particle size, given the sedimentation time. To calculate the fractional mass, the signal is divided by Q_{ext}, (see (1)), which approaches zero at long times. In the case of fractions below 20 nm, the extinction efficiency is close to zero [32]. Consequently, a nonlinear drift in the baseline gives a significant change in the calculated mass fraction for very small particles and is amplified significantly in the PSDs for particles in this size range. Therefore, the slight increase

of mass between 10 nm and 20 nm cannot conclusively be attributed to a fraction of small nanoparticles (Figures 1, 2, 3, 4, and 5). This is supported by SEM micrographs of the suspensions, which did not reveal a mass fraction of very small particles.

It is expected that the transmittance of CNT suspensions decreases with sonication time, as the number of particles in the liquid increases. This has been used as a measure of the quality of the dispersion [30, 37]. We see the same trend in the PSDs from the ultrasonic bath (Figure 1). The transmittance decreased, as the number density of particles, due to fragmentation of agglomerates, increased with sonication time. However, not only the particle density, but also the total mass in the size range from 10 nm–2 μm increased with sonication time. Agglomerates larger than 2 μm cannot be detected at this running condition in the DCF. Particles larger than 2 μm will break up into smaller ones and the concentration of these larger particles is not insignificant at shorter sonication times.

The flow-through horn sonicator can be used to investigate the effects of higher-energy sonication. At the lowest setting of 10%, the sonication was mild and had a low-power output of 10–15 W. The results, see Figure 2, are comparable to the ultrasonic bath, although it seems that even at this low energy output, the dispersion is better, when comparing corresponding treatment times. Increasing the amplitude setting to 20%, as shown in Figure 3, led only to a small increase in the quality of the dispersions. This is somewhat surprising, because larger amplitudes mean larger displacements of liquid, steeper pressure changes, and therefore a higher volume of cavitation [38]. If cavitation is the main process in the exfoliation of the CNTs, increasing the amplitude should have a more pronounced, positive effect on the dispersability.

Increasing the amplitude to 40% and higher, on the other hand, led to significant changes in particle size distributions, as shown in Figure 4 (40%) and Figure 5 (70%). At 40% tip amplitude, the dispersion was significantly better at comparable sonication times. However, PSDs of experiments at large amplitudes and longer times showed deviation from the previously observed bimodal behaviour. In the experiments at 70%, the amount of free CNTs in the PSDs appeared to decrease with increasing sonication time and the bimodal shape was lost at longer times. At increasing times the mode of the emerging monomodal distribution was also shifted to larger particles compared to the free, exfoliated nanotubes. Sonochemical reactions of some of the constituents, associative effects, nanotube damage, or reagglomeration are some of the possible explanations for this behaviour. Thermogravimetric analysis and SEM imaging were performed to check for possible explanations. These results are discussed in Section 3.2.

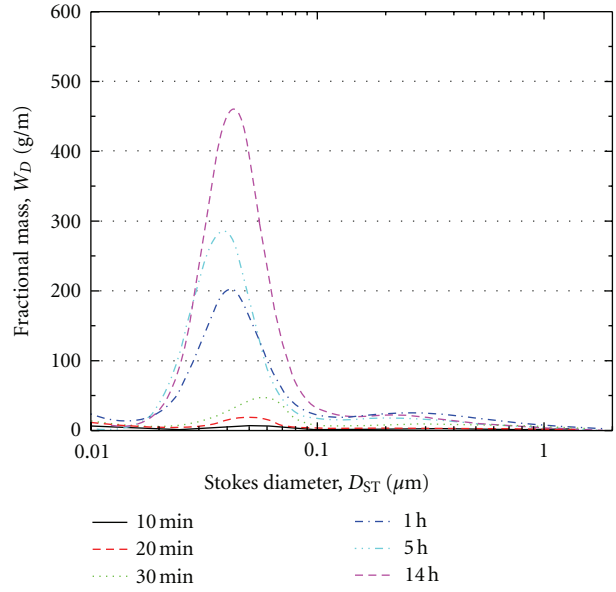

Figure 2: Particle size distributions of Arkema CNTs with increasing sonication time using a horn sonicator with flow cell at 10% amplitude.

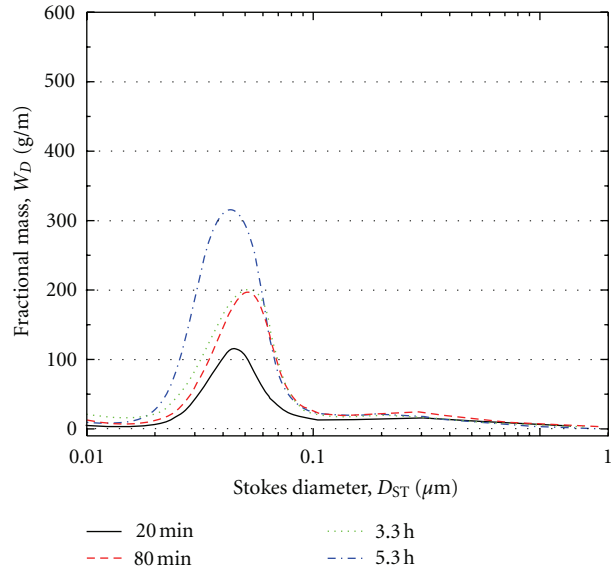

Figure 3: Particle size distributions of Arkema CNTs with increasing sonication time using a horn sonicator with flow cell at 20% amplitude.

3.1. Time Dependence. As discussed above, the total mass increases markedly with sonication time during low-intensity sonication, both for the bath sonicator and the tip sonicator at low amplitude. By integrating the PSDs, two particle mass parameters were determined. These are W_{CNT}, which is the particle mass in the dispersion ranging from 20 nm to 100 nm and W_{OBS}, the total mass in the size range from 20 nm to 2 μm. In general, W_{OBS} should increase and approach a constant value, determined by the CNT concentration in the suspension, if the sonication is effectively dispersing particles larger than 2 μm. Moreover, the ratio W_{CNT}/W_{OBS} gives the mass fraction of exfoliated CNTs in the same manner as the cumulative weight distribution used by Nadler et al. [28] and is denoted as the *degree of exfoliation*.

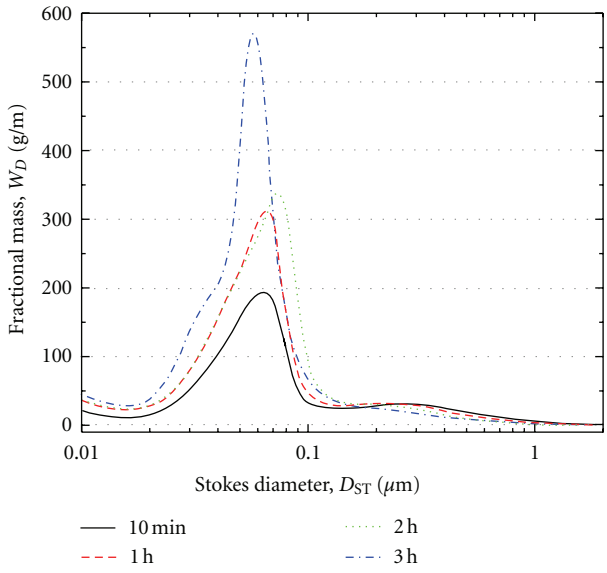

Figure 4: Particle size distributions of Arkema CNTs with increasing sonication time using a horn sonicator with flow cell at 40% amplitude.

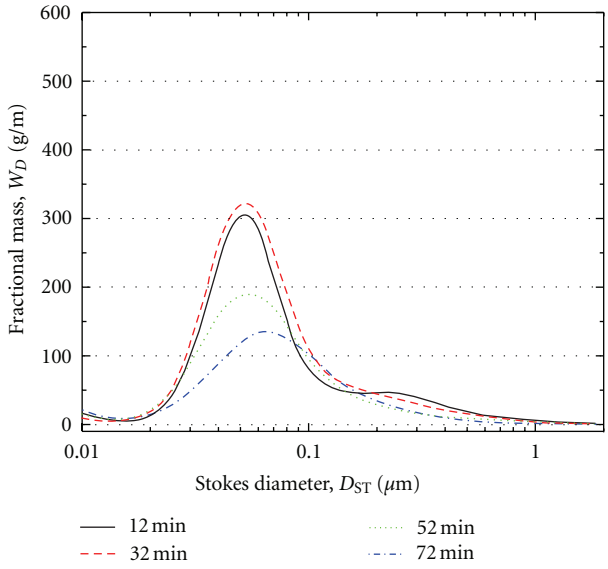

Figure 5: Particle size distributions of Arkema CNTs with increasing sonication time using a horn sonicator with flow cell at 70% amplitude.

The amount of exfoliated CNTs increases slowly with time in the bath sonicator and a plateau is reached after a few hours, see Figure 6. The horn sonicator is more efficient than the bath, but equilibrium is not reached within the time frame of the experiments. At short and intermediate times, that is, the first hour, the mass of freely dispersed carbon nanotubes is comparable for the bath sonicator and the horn sonicator at the lowest setting of 10%. At longer times, the tip sonicator has the ability to produce better dispersions, even at the lowest power input. The same increase of W_{CNT} against

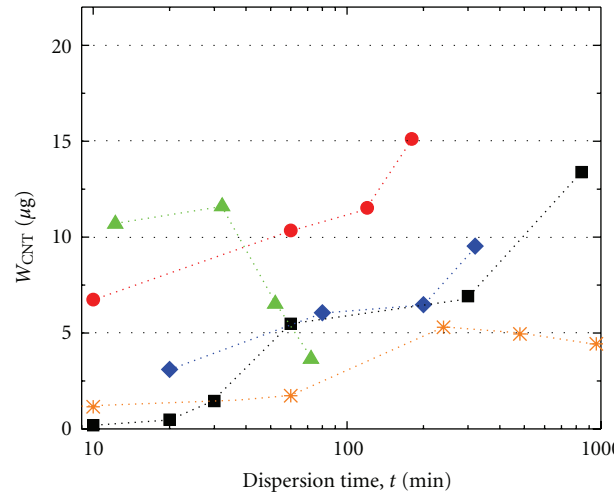

Figure 6: Mass of CNTs in the suspension, W_{CNT}, as a function of sonication time and horn amplitude: 10% (■), 20% (♦), 40% (•), 70% (▲), and bath sonicator (∗).

time, apparently a log-linear relationship, was observed for the 20% and 40% case. Increasing the amplitude up to 40% had a clear effect on the rate of dispersion, as comparable amounts of CNTs were exfoliated in a tenth of the time compared to the 10% case. In the PSDs at 70%, see Figure 5, there is an evident broadening in the particle size distribution of the mass fraction of CNTs with increasing sonication time. At 72 minutes, the PSD is close to monomodal, ranging from 20 nm to 1 μm. Discussion of the particle mass, W_{CNT}, in the same way as in the other experiments is not relevant in this case, because the distribution is much broader than the mass fraction from 20–100 nm used to calculate W_{CNT}. A distinction between exfoliated and agglomerated CNTs is not possible in the PSDs. The dataset at 70% is included in Figure 6 to Figure 8 for comparison, but is omitted in later figures.

Not only the mass of exfoliated CNTs, but also the total observed mass (Figure 7), increased with sonication time. The increase is clearly dependent on the sonication intensity. For the bath sonicator and the horn sonicator at the 10% setting, the increase is significant up to a dispersion time of around 400 minutes. For the 40% amplitude the maximum observed mass was higher and nearly constant after only 10 minutes. An even higher mass was reached at 70% (after 20 minutes), but decreased markedly at longer times. This indicates that there are large strongly bound agglomerates that need high-intensity sonication to be broken, and that the breakup of these large agglomerates is a quick process at high-intensities. This is similar to observations using high-pressure homogenization, where the first pass through the homogenizer is the most significant in breaking the agglomerates [25]. However, at such high-sonication intensities, undesired side effects or CNT breakage may occur during the sonication treatment (see below) [18].

The log-linear increase of W_{CNT}/W_{OBS} with dispersion time is seen for all of the experiments, except at 70% (Figure 8). The mass of exfoliated CNTs, W_{CNT}, increases even

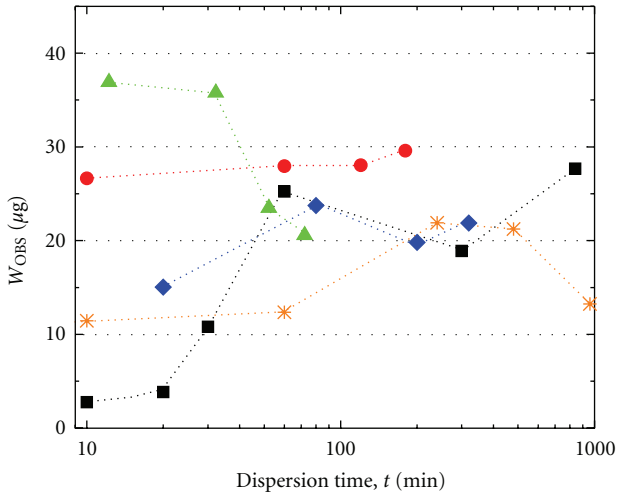

FIGURE 7: Total detected mass between 20 nm and 2 μm, W_{OBS}, as a function of sonication time and horn amplitude: 10% (■), 20% (♦), 40% (•), 70% (▲), and bath sonicator (∗).

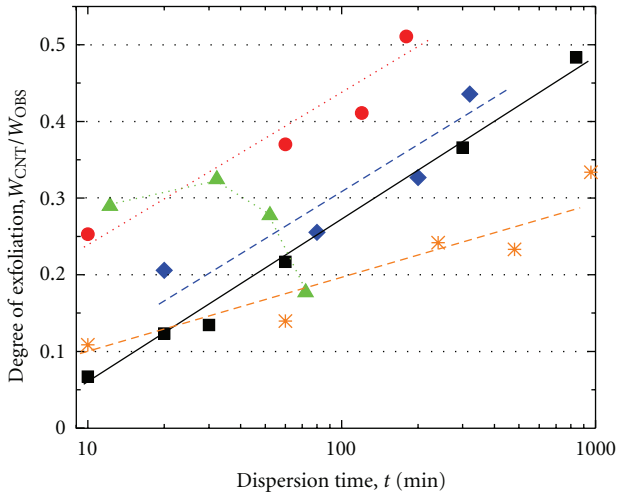

FIGURE 8: Mass fraction of CNTs relative to the total observed mass in suspensions, W_{CNT}/W_{OBS}, as a function of sonication time and horn amplitude: 10% (■), 20% (♦), 40% (•), 70% (▲), and bath sonicator (∗). The straight lines are guides to the eye.

when W_{OBS} is constant, as seen in the measurements at 40%. Therefore, there must be an exfoliation of CNTs from these smaller agglomerates over time. The intensity of the sound field is high enough to break up these agglomerates, even at 10% amplitude, but the rate of the dispersion is low unless the sonication intensity is high. The degree of exfoliation was approximately 50%, so there is clearly room for improvement in the dispersion procedure. Further optimisation of the dispersion process by changing the flow cell geometry and temperature, or using diluents, should probably be possible.

3.2. High-Power Sonication. Dispersions at 70% tip amplitude did not give the typical bimodal PSDs at sonication

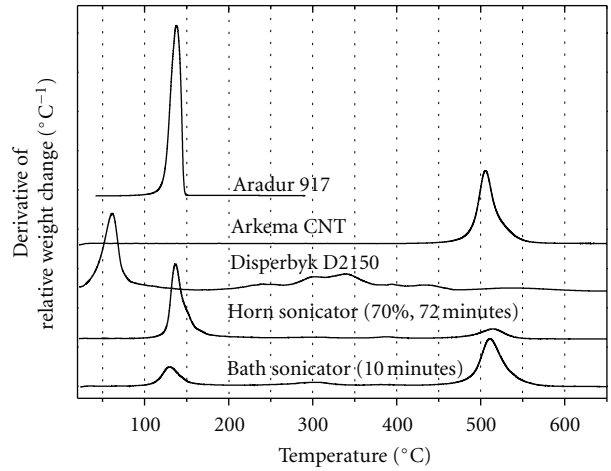

FIGURE 9: Thermogravimetric analysis of two suspensions and reference samples. The curves have been shifted on the Y-axis for better clarity. The reference samples were measured as received. The polymer stabilizer (D2150) was dissolved in a solvent by the supplier, and the large mass loss at 70°C is due to evaporation of this solvent.

times of 32 minutes and above, as can be seen in Figure 5. We believe that at this high energy input, other processes in addition to pure cluster break-up are taking place, and we have given this phenomenon some consideration, as described below: all of the constituents in the dispersion were examined with TGA, as shown in Figure 9. A sample that is sonicated for 72 minutes at 70% was compared to the same type of dispersion treated for only 10 minutes in the bath sonicator. The sample preparation (by centrifugation) showed significant differences between these samples. The sample from the bath sonicator revealed a dry powder as is normal for nanotubes, however, in the 70% case, the nanotubes were embedded in a viscous phase after the purification procedure. This paste was poorly dissolved in MIBK, compared to dispersions at lower intensities, which are easily dissolved in MIBK. The TGA measurements did not reveal any significant shift in the decomposition temperatures of the CNTs, but the purified sample from the 70% case did contain a significantly larger amount of MTHPA, compared with the purified sample from the bath sonicator. Scanning electron micrographs revealed that the CNTs were indeed embedded in a viscous medium. The TGA experiments showed that MTHPA decomposes below 150°C, and heating the sample prepared for the SEM to 200°C for 48 h, removed the viscous phase, as seen in Figure 10. The sample was heated above the decomposition temperature of MTHPA, but below that of D2150, and therefore, MTHPA is most likely the primary substance of the viscous phase.

It may be thought that at very high energy input, the CNTs themselves may be damaged, and therefore, the CNTs were checked for sonication damage (Figure 11). Severe damage was not evident in the SEM images, even at long sonication times at high-power. We therefore believe that the broad monomodal PSDs seen in Figure 5 are probably related to a sonically or thermally induced reaction of the anhydride in the dispersion. Since MIBK was a poor solvent for the

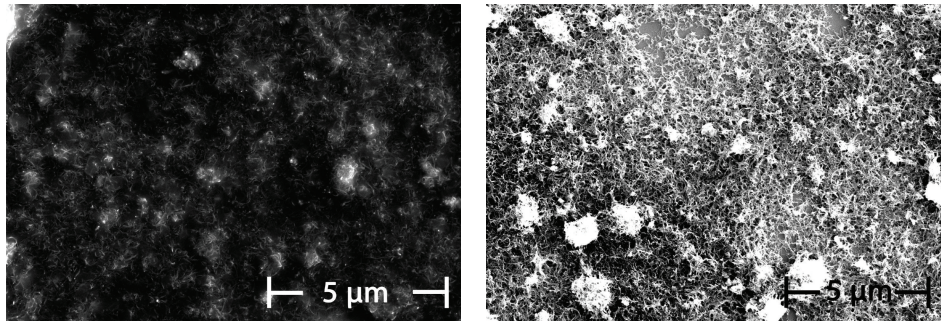

(a) (b)

Figure 10: Scanning electron micrographs of the MWCNTs after TGA sample preparation. MWCNTs dispersed at 70% for 72 min (a) and the same specimen heated to 200°C for 48 h (b).

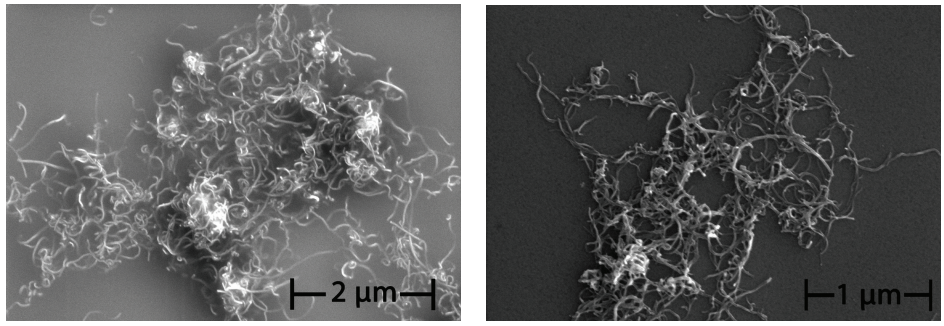

(a) (b)

Figure 11: Scanning electron micrographs of the MWCNTs after TGA sample preparation. MWCNTs dispersed 10 min in a bath sonicator (a) and at 70% for 72 min (b).

mentioned viscous phase, the dilution step before injection in the DCF was probably not very effective, and is a likely reason for the observed PSDs at 70% tip amplitude. This means that the acid anhydride is not stable in sonication at 70%, and that the abnormalities in the PSDs could be caused by this viscous phase entangling the nanotubes. Apart from these considerations; we have not seen it as timely to investigate these side effects further in this work.

3.3. Specific Energy Input. The sonicator control electronics reports the energy consumption of the transducer while keeping constant amplitude of the resonating horn. This can be used to estimate the specific energy input to the suspension. In Figure 12, the power consumption is plotted as a function of the amplitude. The relationship between the power consumption and tip amplitude is linear in the amplitude range from 10% to 40%. The conditions were less reproducible at 70% and more energy was needed, comparably, to keep constant amplitude. The small confined space of the flow cell may give excessive damping of the horn resonance at large amplitudes. Larger amplitudes than 70% were not possible with the attached flow cell, because the instrument could not establish a resonance in the horn. The flow cell was constructed with the inlet straight beneath the horn tip and the suspension was pumped through a ceramic orifice fixed a short distance from the tip (0.8 mm). The high-intensity sound field was mainly focused at this small volume of approximately 0.5 mL. At 10% amplitude, the power throughput is around 15 W, which gave a very intense sonication of 30 W/mL. In comparison, the bath sonicator had a total power of around 270 W dissipated into a volume of 2 L. This equals a much less intense sonication treatment of 0.14 W/mL. The resulting specific energy input of the bath is 0.5 kJ/mL per hour. Even though the specific power at the horn tip is high, the suspension resides in the sonicator's acoustic field only for a fraction of the treatment time. The suspension is circulated through the flow cell, and the total volume was 100 mL in all of the experiments. The specific energy input in the flow cell at 10% was therefore also 0.5 kJ/mL per hour.

The power consumption changed very little over time in these experiments, which led to a linear relationship between energy input and sonication time. Consequently, the same trends in W_{CNT} and W_{OBS} can be seen when plotted as a function of total energy input, E_{US}, as shown in Figure 13. Bath sonicator experiments are plotted in the same figure as a reference. To compare the data from the two sonicators, the estimated specific energy dissipation, 0.5 kJ/mL per hour, of the bath sonicator was used to calculate an energy input in the sample.

Up to 40% amplitude, a higher-intensity sonication is more effective at exfoliating CNTs at comparable energy

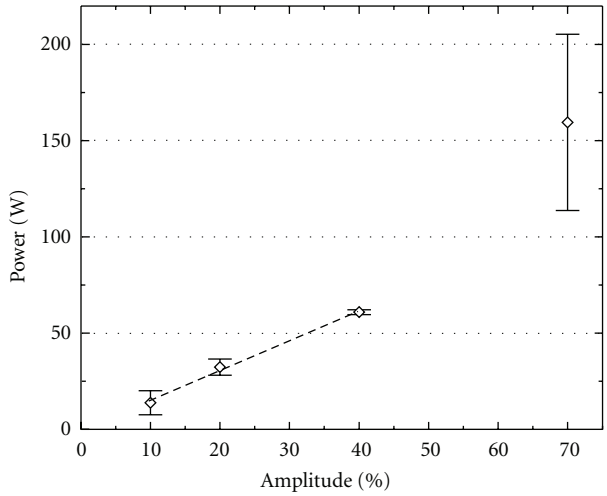

FIGURE 12: Horn transducer power consumption as a function of tip amplitude.

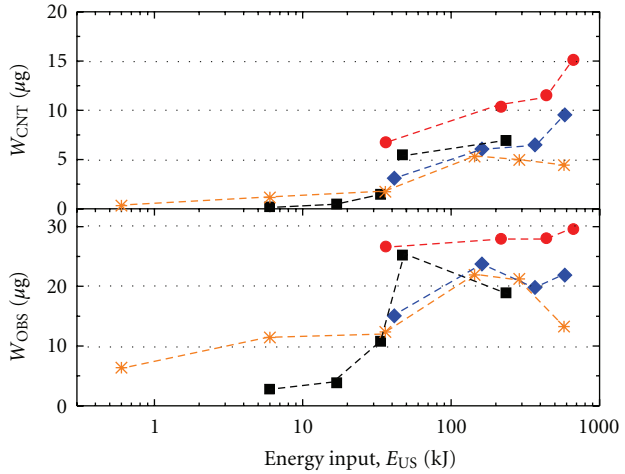

FIGURE 13: Mass of CNTs in the suspension, W_{CNT}, (upper graph) and the total detected mass between 20 nm and 2 μm, W_{OBS}, (lower graph) at increasing energy input, E_{US} at different horn amplitudes: 10% (■), 20% (♦), 40% (•), and bath sonicator (∗).

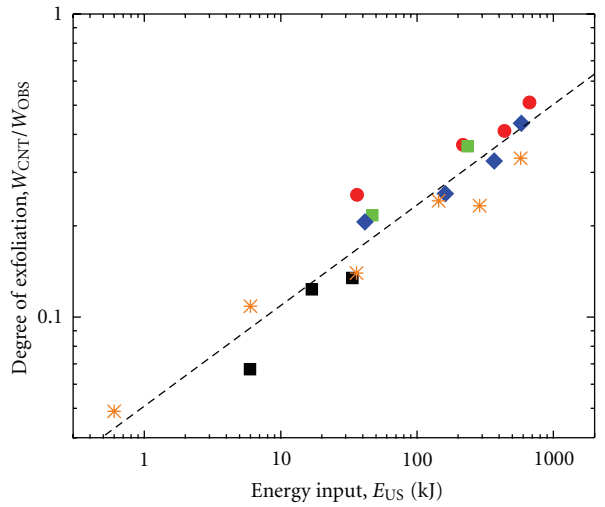

FIGURE 14: Mass fraction of CNTs relative to the total observed mass fraction in suspensions, W_{CNT}/W_{OBS}, at increasing energy input and different horn amplitudes: 10% (■), 20% (♦), 40% (•), and bath sonicator (∗). Dashed line, $y = 0.05x^{0.33}$, shows a nonlinear curve fit of the data.

inputs. The same is true for breaking large particles/agglomerates into smaller ones below 2 μm. Most noteworthy is that the relative mass of CNTs showed a power law dependency with the energy input, as shown in Figure 14. A nonlinear curve fit showed the scaling to be $W_{CNT}/W_{OBS} \sim E_{US}^{0.33}$.

Nadler et al. [28] investigated bath sonication of Baytubes C150P MWCNTs in water. If we assume their sonicator bath was filled to the recommended volume, the specific energy input should be 0.7 times the one used in this work. From [28], the relative exfoliation of Baytubes C150P in an aqueous suspension scales well with $\sim E_{US}^{0.4}$ up to at least 50% exfoliation. However, the Baytubes CNTs in aqueous suspension reached a much higher degree of exfoliation than the Arkema CNTs in MTHPA reported in this paper, at least within the experimental time frame. Naturally, the power law dependency breaks down as the CNTs approach 100% exfoliation. It cannot be concluded that there is a true power law dependency from these data alone [39].

Hennrich et al. [40] used atomic force microscopy (AFM) to show that the length (L) of single-walled nanotubes decreased with $L \sim t^{0.5}$(constant power) (where t is time). Lucas et al. [18] found, with dynamic light scattering, similar results for multiwall nanotubes. In their case, a slower decrease of $L \sim E_{US}^{0.2}$ was observed. An optimum dispersion of carbon nanotubes is achieved when the amount of agglomerates is minimised, while the aspect ratio of the CNTs is retained. The above mentioned works indicates that there is a trade-off between the level of dispersion and sonically induced damage, when conventional sonication is used. Sonication schemes should be adjusted according to the intended usage of the dispersions. For good electrical conductivity, a high aspect ratio is probably more important than small amounts of agglomerate residues. As mechanical reinforcements, these agglomerates could be critical, ultimately weakening the composite. Significant reinforcement has been demonstrated at particle loading levels below 1% (w/w) [41]. At higher loadings, the strength tends to go down, possibly because of an increased number of agglomerates.

3.4. Mechanisms of Separation. Fragmentation theory describes the processes of breaking particles into smaller constituents. A thorough treatment of dispersion mechanisms in the context of fragmentation theory has been given by, for example, Cheng and Redner [42]. They make a clear distinction between agglomerates and aggregates. Agglomerates consist of a number of aggregates and can break up during a typical dispersion process. Aggregates, for example, primary particles or small crystals, are the smallest possible particles produced in the dispersion process. Further fragmentation of these particles does not occur during the dispersion process.

In our case, the primary particle would be the exfoliated nanotube, but as noted earlier, further fragmentation of CNTs, that is, nanotube breakage, can happen in a typical dispersion scheme [2, 18, 19, 22, 43].

In a continuous fragmentation process, the particle concentration, $c(x,t)$, of particles with mass x at time t can be expressed by

$$\frac{\partial c(x,t)}{\partial t} = -a(x)c(x,t) + \int_x^\infty c(y,t)a(y)f(x \mid y)dy. \quad (2)$$

Here, $a(x)$ is the fragmentation rate of particles of mass x, and $f(x \mid y)$ is a relative fragmentation rate, given by the conditional probability of a breakup event where a particle of mass x is produced from a larger particle of mass y [42, 44, 45]. Depending on the dispersion process, different fracture phenomena may occur, and three characteristic regimes can be defined as (1) *rupture* (or cleavage), (2) *erosion* (or abrasion), and (3) *shattering* (or destructive breaking). Ottino et al. [45] introduced a dimensionless parameter characterising the fragmentation process similar to the well-established capillary number (Ca) which is useful in the discussion of the above-mentioned fracture regimes. This *fragmentation number* (Fa), is the ratio between the viscous shear stress and the strength of the agglomerated particles

$$\mathrm{Fa} = \frac{\mu\dot{\gamma}}{T}, \quad (3)$$

where μ is the viscosity, and $\dot{\gamma}$ is the shear rate. Furthermore, T quantifies the cohesive strength, analogous to the surface tension for a droplet. In shear flow dispersion, Fa increases with the energy input. At sufficient energy inputs, then $\mathrm{Fa} > \mathrm{Fa}_{\mathrm{critical}}$, and the liquid shear stress exceeds the cohesive strength of the agglomerates. This results in a rupture of the original particle into two or more particles of similar size. At $\mathrm{Fa} < \mathrm{Fa}_{\mathrm{critical}}$, fragmentation can still occur. Erosion is then the main mechanism of dispersion, where small (primary) particles detach from the surface of the mother particle. Erosion can be a significant effect when the agglomerates consist of discreet primary particles, such as carbon nanotubes, and the resulting particle size distribution is bimodal [28]. Erosion and cleavage are extremes on a continuous scale of fracture. The distinction between these processes is given (arbitrarily) in different ways in the literature. Rwei et al. [46] defines erosion as rupture with child particles of less than 10% of the volume of the mother particle, while Ottino et al. [45] use the term more loosely about fragmentation when $\mathrm{Fa} > \mathrm{Fa}_{\mathrm{critical}}$. It should be stressed that erosion can be significant even when rupture is the dominating process [47]. Erosion is, in nature, a surface effect, and rupture of larger particles will create fresh surfaces which subsequently can undergo erosion. Recently, Kasaliwal et al. [48, 49] have studied the effects of erosion and rupture processes for CNT suspensions in polycarbonate (PC). By the use of a microcompounder, the share rate could be varied to separate the two effects.

As stated earlier, $a(x)$ in (2) is the rate of fragmentation. In a homogenous fragmentation process, $a(x) \sim x^\lambda$, where λ is the *homogeneity index* [44]. In the most common case,

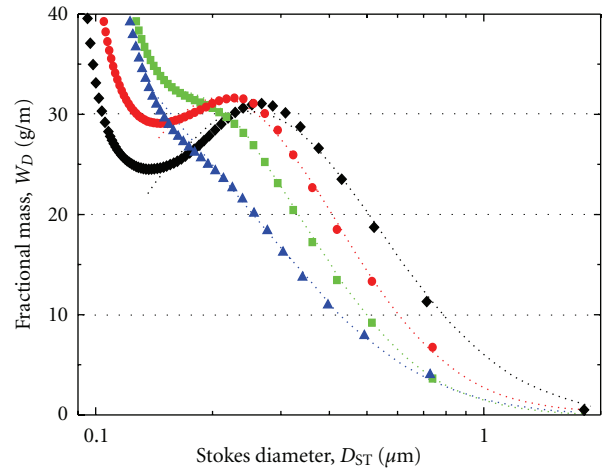

FIGURE 15: Particle size distributions of CNTs (symbols) at different sonication times at 40% tip amplitude: 10 min (♦), 1 h (•), 2 h (■), and 3 h (▲). The dotted lines show the corresponding fitted log-normal distributions.

λ is positive, and the rate of fragmentation due to rupture will decrease with particle size (mass). At the same time, the number of particles, and also the surface area, increases with rupture. In total, erosion should become more prominent, relative to rupture, as dispersion time increases, and consequently the size of the particles decreases. If λ is negative, shattering occurs. In this case, the rate of fragmentation will increase with decreasing particle size, and mass "vanishes" from the observed PSD as the agglomerates shatters into infinitesimally small particles. Equation (2) has been analyzed for different fragmentation phenomena, but mainly for rupture.

If "mother particles" break into random-sized particles through a stochastically determined process (Markov process), the final distribution will be log-normal in the limit of small particles, as first shown in the theory of Kolmogorov [50]. For the MWCNTs in this study, the initial agglomerate size is 10–1000 μm [26]. After prolonged sonication, the agglomerates in the size range from 0.1–2 μm exhibited a particle size distribution approaching a log-normal shape, as seen in Figure 15, indicating a rupture mechanism even though the bimodal shape of the PSDs clearly suggests an erosion-like behaviour of the MWCNTs. The agglomerate size distribution indicates that both erosion-like and rupture-like breakup events occur.

Further sonication did not change the general log-normal shape of the distribution, even though the average agglomerate size decreased. This self-similarity is predicted by the Kolmogorov model. Hansen et al. [44] argue that the average agglomerate size, s, scales with time as

$$s(t) \sim t^{-1/\lambda}, \quad (4)$$

where λ is the previously mentioned homogeneity index. Equation (4) holds for rupture-like breakup events with positive values of λ [51]. The parameter s is estimated as the mean value from the fitted log-normal distributions, as seen in Figure 15. At long sonication treatments, a power law

Table 1: Exponents of fitted data to (4) as shown in Figure 16.

Experiment	$-1/\lambda$	λ
10%	−0.24	4.13
20%	−0.24	4.17
40%	−0.27	3.72
Bath	−0.24	4.09

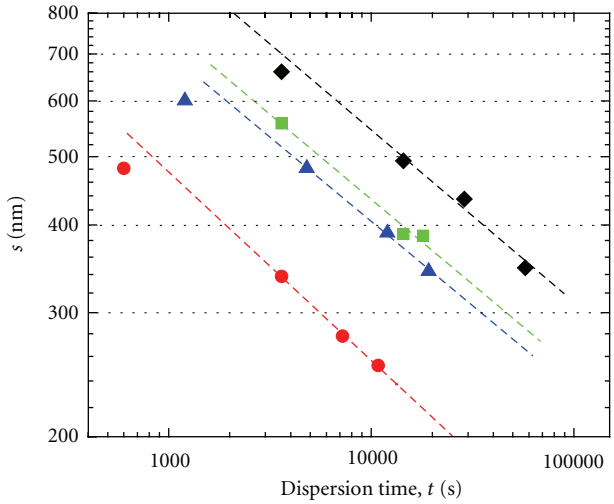

Figure 16: Mean agglomerate size data from fitted log-normal functions as a function of sonication time, t, at different tip amplitudes: 10% (■), 20% (▲), 40% (•), and bath sonicator (♦). For each tip amplitude, the three longest times were used to fit (4).

dependence, as given in (4), was observed (see Figure 16 and Table 1). The time dependence of the mean agglomerate size is very similar for the lowest tip amplitudes and for the bath. The fitted parameter, λ, is ranging from 4.09 to 4.17. Consequently, the rate of fragmentation is similar in these experiments. At 40% amplitude, a slightly lower value of 3.72 is found. A lower value of λ indicates that the fragmentation rate is less dependent on the particle size. It could be that the higher share rate increases the probability of rupture of much smaller agglomerates than at the lower amplitudes. At sufficiently high share rates, the probability of rupture is constant for particles of any size, because all particles will break, irrespective of size. Consequently, the homogeneity index will be zero in this case. A lower value of λ is therefore expected when the acoustic power of the sonicator increases.

Power law behaviour has also been described without the use of fragmentation theory. Bittmann et al. [52] correlated the size of dispersed TiO_2 nanoparticles to the power input of a tip sonicator,

$$s(t) \sim P_v^{-b_1} \cdot t_v^{-b_2} \approx (P_v \cdot t_v)^{-b}, \tag{5}$$

where P_v is the power input in the cavitation zone, and t_v is the mean residence time in the same zone. In the current setup, this cavitation zone is between the ceramic orifice and the sonicator tip inside the flow cell. If the right hand side of (5) holds, we can rewrite it as

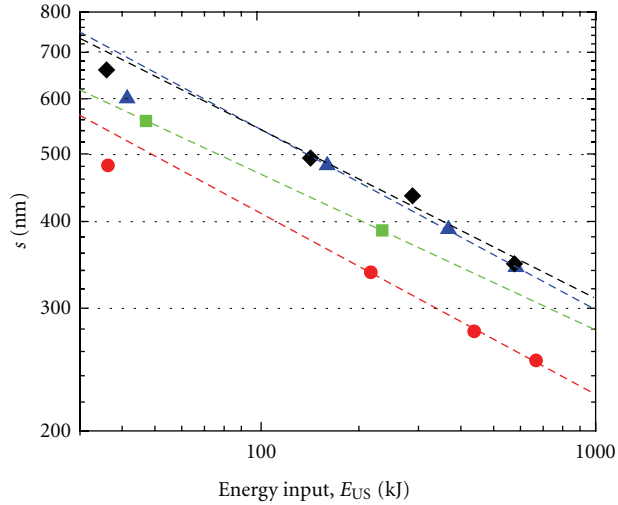

Figure 17: Mean agglomerate size data from fitted log-normal functions as a function of sonication energy input, E_{US}, at different tip amplitudes: 10% (■), 20% (▲), 40% (•), and bath sonicator (♦). For each tip amplitude, the same datasets as in Figure 16 were used to fit (6).

$$s(t) \sim E_{US}^{-b}, \tag{6}$$

where E_{US} is the energy input from the tip sonicator, given the energy input scales with the cavitation activity inside the flow-cell cavitation zone. The same data set as seen in Figure 16 was fitted against the energy input, E_{US}. The data is well described by the volume based model in (6), as seen in Figure 17.

The data shows approximately the same scaling relationship with the average agglomerate diameter as a function of sonicator energy input. However, the dispersion of the agglomerates is both faster at 40%, than in the experiments with less intense sonication (see Figure 16), and the process is also much more energy efficient (Figure 17). This suggests that the initial breakup of the large agglomerates is dependent on the sonication power, but that the further dispersion process is more dependent on the total energy input.

A model, where the particle erosion is proportional to the particle surface and applied shear was proposed by Kao and Mason [53] and later developed and investigated by others [44, 46, 54]. Instead of a power law dependency, an exponential decay with time is expected, as seen in Equation (7):

$$s(t) \sim s_0 e^{(-K\dot{\gamma}t)} + c, \tag{7}$$

where s is the average agglomerate size and s_0 the initial size of the agglomerates. $\dot{\gamma}$ is the applied share rate, c is an integration constant, and K is a constant dependent on factors such as the type of flow, agglomerate strength, and the liquid shear stress [46]. This exponential relationship is similar to the model used by Kasaliwal et al. [49]. They showed that the size of agglomerates in the range from 1–10 μm decreased

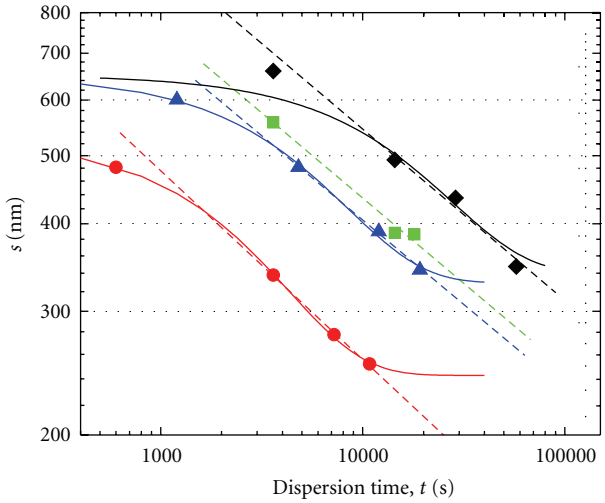

FIGURE 18: Agglomerate size data at 20% and 40% amplitude were fitted using (4) (dotted lines), and (7) (solid lines). Marquardt nonlinear curve fit did not give converging results for the other two datasets. Eqution (7) was plotted with estimated parameters as a guide for data from the bath sonicator. Amplitudes 10% (■), 20% (▲), 40% (•), bath sonicator (♦).

exponentially over time and attributed this to an erosional dispersion of CNT agglomerates.

Average agglomerate size data from our experiments was fitted to (7), and the results are given in Figure 18.

Convergent results were obtained from experiments at 20% and 40% tip amplitude. At short sonication times, the agglomerate size distribution did not correspond well to a log-normal distribution. Consequently, the estimated average size, s, was not well estimated at short times at low-energy input. Still, (7) could be plotted for the bath sonicator series, with estimated parameters. As seen in Figure 18, both a power law dependency and an exponential decay fit these data sets reasonably well. As previously mentioned, both erosion and rupture are likely to occur in this kind of experiment, but conclusive information about the dominating process of fragmentation could not be drawn from these datasets. From a physical point of view, erosion is a likely process for CVD type MWCNTs. Agglomerates are highly entangled, and the cohesive strength of the primary particles are very large compared to the particle-particle interaction. An erosion-type dispersion will probably lead to less damage to the tubes than a dispersion process where rupture is the dominating fragmentation event.

4. Summary

Ultrasonic dispersion of carbon nanotubes was investigated. 1% (w/w) of MWCNT in a commercially available curing agent was dispersed using both a bath sonicator and a horn sonicator with a flow cell attachment at different horn tip amplitudes. Subsequently, suspensions of CNTs were characterized using a disc centrifuge. The horn sonicator was shown to be superior to the low-power bath sonicator, achieving much better dispersions within reasonable sonication times.

Particle size distributions showed a broad bimodal distribution of CNTs in the suspension. The lower-sized mode is attributed to freely suspended nanotubes, and the broader mode at larger particle sizes to agglomerate CNTs. Increasing the dispersion time or acoustic intensity of the sonication had a positive effect on the quality of the dispersion, by increasing the mass fraction of the free, un-entangled nanotubes. However, at 70% tip amplitude, unwanted side effects were detected. SEM and TGA investigations indicated that a sonochemically induced reaction with the anhydride occurred. Therefore, optimal horn tip amplitude of approximately 40% was found as a compromise between rate of dispersion and minimizing side reactions in the suspension.

The relative mass fraction of unentangled CNTs compared to the total mass of CNTs observed in the PSD was estimated and denoted as the degree of exfoliation in accordance with earlier works. This mass fraction increased with sonication time with a log-linear behaviour. Increasing the tip amplitude (energy input) gave a higher degree of exfoliation, but approximately the same log-linear increase with time was observed for all of the horn sonicator experiments. The relative mass of CNTs increased much slower in the bath sonicator, reaching only 30% exfoliation after 16 h.

The energy input from the sonicators was correlated to the degree of exfoliation, and the data showed a strong power law dependency condensing onto the same master curve. The degree of exfoliation increased with the energy input with an exponent of 0.33 in all of the dispersion experiments. We conclude that the quality of the dispersion was controlled by the total energy input, and that a sufficiently intense acoustic sound field is needed to efficiently produce dispersions of good quality

The size distribution of agglomerates showed a strong log-normal shape at longer sonication times, indicating that the larger agglomerates broke into smaller ones in a rupture process. However, the mean agglomerate size, s, was estimated and fitted to three different models. A power law behaviour both with the energy input and sonication time, showed that s scaled well with both time and energy input. Furthermore, a model for erosional particle fragmentation, with an exponential decrease in agglomerate size, fitted the data reasonably as well.

The disc centrifuge can be used to reliably study the evolution of the dispersion process during sonication. Both the amount of unentangled CNTs and parts of the agglomerate size range can be estimated with this technique. A detailed analysis of the size distribution is of vital importance to understand these processes and to be able to evaluate the optimum conditions for the dispersion of CNTs in liquids.

Acknowledgments

The authors would like to acknowledge Mette Grorud for assistance with the sonication experiments, Tomas Lunde Jensen (FFI) for help with the TGA measurements, and Dr. Tom Thorvaldsen, Dr. Bernt Brønmo Johnsen (FFI), and Dr. Marc Steinmetz (CPS instruments) for valuable discussions. The authors of this contribution do not have any direct

financial relation with any commercial identities mentioned in the paper that might lead to a conflict of interest for any of the authors.

References

[1] S. Iijima, "Helical microtubules of graphitic carbon," *Nature*, vol. 354, no. 6348, pp. 56–58, 1991.

[2] J. Hilding, E. A. Grulke, Z. G. Zhang, and F. Lockwood, "Dispersion of carbon nanotubes in liquids," *Journal of Dispersion Science and Technology*, vol. 24, no. 1, pp. 1–41, 2003.

[3] P. X. Hou, C. Liu, and H. M. Cheng, "Purification of carbon nanotubes," *Carbon*, vol. 46, no. 15, pp. 2003–2025, 2008.

[4] D. L. Shi, X. Q. Feng, Y. Y. Huang, K. C. Hwang, and H. Gao, "The effect of nanotube waviness and agglomeration on the elastic property of carbon nanotube-reinforced composites," *Journal of Engineering Materials and Technology, Transactions of the ASME*, vol. 126, no. 3, pp. 250–257, 2004.

[5] A. Godara, L. Mezzo, F. Luizi et al., "Influence of carbon nanotube reinforcement on the processing and the mechanical behaviour of carbon fiber/epoxy composites," *Carbon*, vol. 47, no. 12, pp. 2914–2923, 2009.

[6] E. J. Garcia, B. L. Wardle, and A. John Hart, "Joining prepreg composite interfaces with aligned carbon nanotubes," *Composites A*, vol. 39, no. 6, pp. 1065–1070, 2008.

[7] J.-H. Du, J. Bai, and H.-M. Cheng, "The present status and key problems of carbon nanotube based polymer composites," *Express Polymer Letters*, vol. 1, no. 5, pp. 253–273, 2007.

[8] R. K. Duncan, X. G. Chen, J. B. Bult, L. C. Brinson, and L. S. Schadler, "Measurement of the critical aspect ratio and interfacial shear strength in MWNT/polymer composites," *Composites Science and Technology*, vol. 70, no. 4, pp. 599–605, 2010.

[9] A. H. Barber, S. R. Cohen, S. Kenig, and H. D. Wagner, "Interfacial fracture energy measurements for multi-walled carbon nanotubes pulled from a polymer matrix," *Composites Science and Technology*, vol. 64, no. 15, pp. 2283–2289, 2004.

[10] A. Martone, C. Formicola, M. Giordano, and M. Zarrelli, "Reinforcement efficiency of multi-walled carbon nanotube/epoxy nanocomposite," *Composites Science and Technology*, vol. 70, no. 7, pp. 1154–1160, 2010.

[11] P. C. Ma, N. A. Siddiqui, G. Marom, and J. K. Kim, "Dispersion and functionalization of carbon nanotubes for polymer-based nanocomposites: a review," *Composites A*, vol. 41, no. 10, pp. 1345–1367, 2010.

[12] S. Azoubel and S. Magdassi, "The formation of carbon nanotube dispersions by high pressure homogenization and their rapid characterization by analytical centrifuge," *Carbon*, vol. 48, no. 12, pp. 3346–3352, 2010.

[13] O. Behrend, K. Ax, and H. Schubert, "Influence of continuous phase viscosity on emulsification by ultrasound," *Ultrasonics Sonochemistry*, vol. 7, no. 2, pp. 77–85, 2000.

[14] K. S. Suslick and G. J. Price, "Applications of ultrasound to materials chemistry," *Annual Review of Materials Science*, vol. 29, pp. 295–326, 1999.

[15] J. Dooher, R. Lippman, T. Morrone, H. Pohle, and D. Wright, "Ultrasonic disintegration of particles," pp. 11–16, 1978.

[16] T. J. Mason and P. L. Lorimer, *Applied Sonochemistry: Uses of Power Ultrasound in Chemistry and Processing*, Wiley-VCH, Weinheim, Germany, 2002.

[17] C. McClory, S. J. Chin, and T. McNally, "Polymer/carbon nanotube composites," *Australian Journal of Chemistry*, vol. 62, no. 8, pp. 762–785, 2009.

[18] A. Lucas, C. Zakri, M. Maugey, M. Pasquali, P. Van Der Schoot, and P. Poulin, "Kinetics of nanotube and microfiber scission under sonication," *Journal of Physical Chemistry C*, vol. 113, no. 48, pp. 20599–20605, 2009.

[19] S. Badaire, P. Poulin, M. Maugey, and C. Zakri, "In situ measurements of nanotube dimensions in suspensions by depolarized dynamic light scattering," *Langmuir*, vol. 20, no. 24, pp. 10367–10370, 2004.

[20] D. W. Schaefer and R. S. Justice, "How nano are nanocomposites?" *Macromolecules*, vol. 40, no. 24, pp. 8501–8517, 2007.

[21] S. H. Kim, W. I. Lee, and J. M. Park, "Assessment of dispersion in carbon nanotube reinforced composites using differential scanning calorimetry," *Carbon*, vol. 47, no. 11, pp. 2699–2703, 2009.

[22] T. Liu, S. Luo, Z. Xiao, C. Zhang, and B. Wang, "Preparative ultracentrifuge method for characterization of carbon nanotube dispersions," *Journal of Physical Chemistry C*, vol. 112, no. 49, pp. 19193–19202, 2008.

[23] G. Ralston, "Introduction to analytical ultracentrifugation," 1992, https://www.beckmancoulter.com/.

[24] B. Krause, G. Petzold, S. Pegel, and P. Pötschke, "Correlation of carbon nanotube dispersability in aqueous surfactant solutions and polymers," *Carbon*, vol. 47, no. 3, pp. 602–612, 2009.

[25] S. Pegel, P. Pötschke, G. Petzold, I. Alig, S. M. Dudkin, and D. Lellinger, "Dispersion, agglomeration, and network formation of multiwalled carbon nanotubes in polycarbonate melts," *Polymer*, vol. 49, no. 4, pp. 974–984, 2008.

[26] B. Krause, M. Mende, P. Pötschke, and G. Petzold, "Dispersability and particle size distribution of CNTs in an aqueous surfactant dispersion as a function of ultrasonic treatment time," *Carbon*, vol. 48, no. 10, pp. 2746–2754, 2010.

[27] F. K. Hansen, "Particle size measurements with a disc centrifuge," in *Particle Size Distribution II*, T. Provder, Ed., pp. 169–183, ACS Symposium Series, Washington, DC, USA, 1991.

[28] M. Nadler, T. Mahrholz, U. Riedel, C. Schilde, and A. Kwade, "Preparation of colloidal carbon nanotube dispersions and their characterisation using a disc centrifuge," *Carbon*, vol. 46, no. 11, pp. 1384–1392, 2008.

[29] J. Mejia, F. Tichelaar, C. Saout et al., "Effects of the dispersion methods in Pluronic F108 on the size and the surface composition of MWCNTs and their implications in toxicology assessment," *Journal of Nanoparticle Research*, vol. 13, no. 2, pp. 655–667, 2011.

[30] L. Zhao and L. Gao, "Stability of multi-walled carbon nanotubes dispersion with copolymer in ethanol," *Colloids and Surfaces A*, vol. 224, no. 1-3, pp. 127–134, 2003.

[31] Q. Li, M. Zaiser, and V. Koutsos, "Carbon nanotube/epoxy resin composites using a block copolymer as a dispersing agent," *Physica Status Solidi (A) Applied Research*, vol. 201, no. 13, pp. R89–R91, 2004.

[32] M. Kerker, *The Scattering of Light*, Academic Press, New York, NY, USA, 1969.

[33] A. Koshio, M. Yudasaka, M. Zhang, and S. Iijima, "A Simple Way to Chemically React Single-Wall Carbon Nanotubes with Organic Materials Using Ultrasonication," *Nano Letters*, vol. 1, no. 7, pp. 361–363, 2001.

[34] A. Koshio, M. Yudasaka, and S. Iijima, "Thermal degradation of ragged single-wall carbon nanotubes produced by polymer-assisted ultrasonication," *Chemical Physics Letters*, vol. 341, no. 5-6, pp. 461–466, 2001.

[35] K. L. Lu, R. M. Lago, Y. K. Chen, M. L. H. Green, P. J. F. Harris, and S. C. Tsang, "Mechanical damage of carbon nanotubes by ultrasound," *Carbon*, vol. 34, no. 6, pp. 814–816, 1996.

[36] P. S. Gill, S. R. Sauerbrunn, and B. S. Crowe, "High resolution thermogravimetry," *Journal of Thermal Analysis*, vol. 38, no. 3, pp. 255–266, 1992.

[37] N. Grossiord, O. Regev, J. Loos, J. Meuldijk, and C. E. Koning, "Time-dependent study of the exfoliation process of carbon nanotubes in aqueous dispersions by using UV-visible spectroscopy," *Analytical Chemistry*, vol. 77, no. 16, pp. 5135–5139, 2005.

[38] T. Hielscher, "Ultrasonic production of nano-size dispersions and emulsions," *European Nano Systems*, pp. 138–143, 2005.

[39] A. Clauset, C. R. Shalizi, and M. E. J. Newman, "Power-law distributions in empirical data," *SIAM Review*, vol. 51, no. 4, pp. 661–703, 2009.

[40] F. Hennrich, R. Krupke, K. Arnold et al., "The mechanism of cavitation-induced scission of single-walled carbon nanotubes," *Journal of Physical Chemistry B*, vol. 111, no. 8, pp. 1932–1937, 2007.

[41] S. G. Prolongo, M. R. Gude, and A. Urena, "Improving the flexural and thermomechanical properties of amino-functionalized carbon nanotube/epoxy composites by using a precuring treatment," *Composites Science and Technology*, vol. 71, pp. 765–771, 2011.

[42] Z. Cheng and S. Redner, "Kinetics of fragmentation," *Journal of Physics A*, vol. 23, no. 7, pp. 1233–1258, 1990.

[43] K. Yang, M. Gu, Y. Guo, X. Pan, and G. Mu, "Effects of carbon nanotube functionalization on the mechanical and thermal properties of epoxy composites," *Carbon*, vol. 47, no. 7, pp. 1723–1737, 2009.

[44] S. Hansen, D. V. Khakhar, and J. M. Ottino, "Dispersion of solids in nonhomogeneous viscous flows," *Chemical Engineering Science*, vol. 53, no. 10, pp. 1803–1817, 1998.

[45] J. M. Ottino, P. DeRoussel, S. Hansen, and D. V. Khakhar, "Mixing and dispersion of viscous liquids and powdered solids," in *Advances in Chemical Engineering*, J. Wei, Ed., vol. 25, pp. 105–204, Academic Press, New York, NY, USA, 1999.

[46] S. P. Rwei, I. Manas-Zloczower, and D. L. Feke, "Characterization of agglomerate dispersion by erosion in simple shear flows," *Polymer Engineering & Science*, vol. 31, no. 8, pp. 558–562, 1991.

[47] S. P. Rwei, I. Manas-Zloczower, and D. L. Feke, "Analysis of dispersion of carbon black in polymeric melts and its effect on compound properties," *Polymer Engineering & Science*, vol. 32, no. 2, pp. 130–135, 1992.

[48] G. Kasaliwal, A. Göldel, and P. Pötschke, "Influence of processing conditions in small-scale melt mixing and compression molding on the resistivity and morphology of polycarbonate-MWNT composites," *Journal of Applied Polymer Science*, vol. 112, no. 6, pp. 3494–3509, 2009.

[49] G. R. Kasaliwal, S. Pegel, A. Göldel, P. Pötschke Petra, and G. Heinrich, "Analysis of agglomerate dispersion mechanisms of multiwalled carbon nanotubes during melt mixing in polycarbonate," *Polymer*, vol. 51, no. 12, pp. 2708–2720, 2010.

[50] A. N. Kolmogorov, "The logarithmically normal law of distribution of dimensions of particles when broken into small parts," *Doklady Akademii Nauk*, vol. 31, pp. 99–101, 1941.

[51] A. F. Filippov, "On the distribution of the sizes of particles which undergo splitting," *Theory of Probability and its Applications*, vol. 6, pp. 275–294, 1961.

[52] B. Bittmann, F. Haupert, and A. K. Schlarb, "Ultrasonic dispersion of inorganic nanoparticles in epoxy resin," *Ultrasonics Sonochemistry*, vol. 16, no. 5, pp. 622–628, 2009.

[53] S. V. Kao and S. G. Mason, "Dispersion of particles by shear," *Nature*, vol. 253, no. 5493, pp. 619–621, 1975.

[54] R. L. Powell and S. G. Mason, "Dispersion by laminar flow," *AIChE Journal*, vol. 28, no. 2, pp. 286–923, 1982.